

MPI/PhT/98-06
TTP98-04
hep-ph/9801432
January 1998

Singlet Polarization Functions at $\mathcal{O}(\alpha_s^2)$

K.G. Chetyrkin[‡] and R. Harlander

*Institut für Theoretische Teilchenphysik, Universität Karlsruhe,
D-76128 Karlsruhe, Germany*

M. Steinhauser

*Max-Planck-Institut für Physik, Werner-Heisenberg-Institut,
D-80805 Munich, Germany*

Abstract

We consider the three-loop singlet diagrams induced by axial-vector, scalar and pseudo-scalar currents. Expansions for small and large external momentum q are presented. They are used in combination with conformal mapping and Padé approximations in order to arrive at results for the polarization functions valid for all q^2 . Results are presented for the imaginary parts which are directly related to physical quantities like the production of top quarks or the decay of scalar or pseudo-scalar Higgs bosons.

PACS numbers: 12.38.-t, 12.38.Bx, 14.65.Ha

I. INTRODUCTION

In the last few years a lot of effort has been devoted to developments of techniques which allow the evaluation of higher order corrections. Of special interest is thereby the evaluation of QCD corrections to two-point current correlators. Their knowledge immediately leads to a variety of important observables like the cross section $\sigma(e^+e^- \rightarrow \text{hadrons})$ mediated by a photon or a Z boson or the decay of a scalar or pseudo-scalar

[‡]Permanent address: Institute for Nuclear Research, Russian Academy of Sciences, Moscow 117312, Russia.

Higgs boson. Whereas at the one- and two-loop level exact results are known (for a review see [1]), until recently at $\mathcal{O}(\alpha_s^2)$ only expansions for large external momentum q respectively small quark mass m were available.

In [2,3] an approach was developed which leads to semi-analytical results for the three-loop polarization functions. The essence of this procedure amounts to the combination of the low- and high-energy analytical data for a polarization function through the use of the conformal mapping and Padé approximation suggested in [4–6].

In a first step it was applied to the non-singlet diagrams induced by external vector, axial-vector, scalar and pseudo-scalar currents [3]. In this paper this procedure will be applied to the corresponding singlet diagrams. They are often also referred to as double-triangle diagrams as the external currents are not connected through the same fermion line. This completes the knowledge of the three-loop current correlators at $\mathcal{O}(\alpha_s^2)$. Thus also the full mass dependence for the inclusive cross sections $\sigma(e^+e^- \rightarrow t\bar{t})$ and the decays of a scalar or pseudo-scalar Higgs boson into quarks is available at this order.

The method used in [3] heavily relies on the fact that the lowest particle threshold for the non-singlet graphs starts at $q^2 = 4m^2$. In contrast to that, the singlet diagrams contain massless cuts. The solution of this problem is described in detail for the axial-vector correlator in Section II. Also the essential ingredients are listed and the approximation procedure is briefly reviewed. Section III describes the treatment of the scalar and pseudo-scalar diagrams and finally results are presented in Section IV. Note that for the vector correlator there are no singlet diagrams at three-loop level according to Furry’s theorem.

II. SINGLET AXIAL-VECTOR CORRELATOR

In this section the ingredients and the procedure for the construction of the Padé approximants of the axial-vector polarization function are presented in detail. The scalar and pseudo-scalar singlet diagrams are discussed in Section III.

Let us start with some definitions. It is convenient to introduce the dimensionless quantities

$$z = \frac{q^2}{4m^2}, \quad r = \frac{s}{4m^2}, \quad x = \frac{2m}{\sqrt{s}}, \quad v = \sqrt{1-x^2}, \quad (1)$$

where \sqrt{s} is the center of mass energy and m is the pole mass of the produced quark. x is a convenient variable in the high energy region and v represents the velocity of the quark. The axial-vector polarization function is defined through

$$\left(-q^2 g_{\mu\nu} + q_\mu q_\nu\right) \Pi^a(q^2) + q_\mu q_\nu \Pi_L^a(q^2) = i \int dx e^{iqx} \langle 0 | T j_\mu^a(x) j_\nu^a(0) | 0 \rangle, \quad (2)$$

with $j_\mu^a = \bar{\psi} \gamma_\mu \gamma_5 \psi$. Only the transversal part $\Pi^a(q^2)$ will be considered in the following. In $D = 4 - 2\varepsilon$ space-time dimensions care has to be taken concerning the treatment of γ_5 — especially in connection with the singlet diagrams. We follow the treatment introduced in [7] and refer for more details to [8].

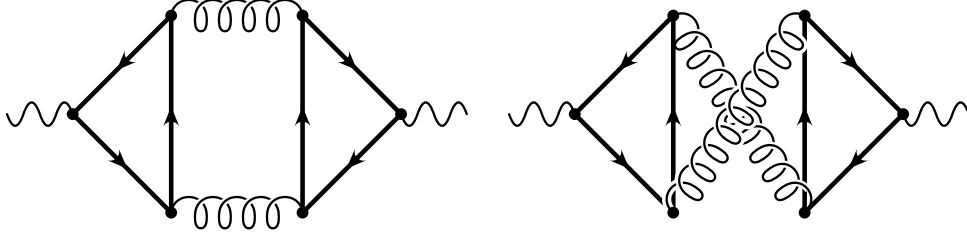


FIG. 1. Singlet or double-triangle diagrams. In the fermion lines either the quark ψ or its isospin partner χ may be present.

In order for the axial anomaly to cancel, one has to take both members of a weak isospin doublet into account. It is therefore convenient to replace the current j_μ^a in Eq. (2) by $j_{S,\mu}^a = \bar{\psi}\gamma_\mu\gamma_5\psi - \bar{\chi}\gamma_\mu\gamma_5\chi$, where ψ and χ are isospin partners. The diagrams contributing to the singlet part, $\Pi_S^a(q^2)$, are depicted in Fig. 1 where in the fermion triangles either ψ or χ may be present. Note that for a degenerate quark doublet $\Pi_S^a(q^2)$ vanishes. Having in mind the physical case $(\psi, \chi) = (t, b)$, however, we set $m_\psi = m$ and $m_\chi = 0$ in the subsequent analysis. $\Pi_S^a(q^2)$ is conveniently written in the form

$$\Pi_S^a(q^2) = C_F T \left(\frac{\alpha_s}{\pi} \right)^2 \Pi_S^{(2),a}(q^2), \quad (3)$$

where $C_F = (N_c^2 - 1)/(2N_c)$, and T is the trace normalization for an $SU(N_c)$ gauge group. For QCD $N_c = 3$ and $T = 1/2$.

The imaginary part of $\Pi_S^a(q^2)$,

$$R_S^a(s) = 12\pi \text{Im} \Pi_S^a(q^2 = s + i\epsilon), \quad (4)$$

normalized in analogy to the vector case, enters, e.g., the total inclusive cross section for the production of top quarks. However, also imaginary parts arising from the massless quark χ contribute to $R_S^a(s)$. The purely gluonic cut is zero according to the Landau-Yang-Theorem [9]. Let $R_{Sb}^{(2),a}$ be the contribution of these massless cuts to R_S^a . Then the quantity

$$\hat{\Pi}_S^a(q^2) = \frac{1}{12\pi^2} \int_0^1 dr \frac{R_{Sb}^{(2),a}(s)}{r - z} \quad (5)$$

defines a function whose imaginary part for $q^2 \leq 4m^2$ coincides with that of $\Pi_S^{(2),a}(q^2)$ and is zero for $q^2 > 4m^2$. Its evaluation will be described below. With the help of this function we choose the overall renormalization condition for $\Pi_S^{(2),a}$

$$\lim_{q^2 \rightarrow 0} \left(\Pi_S^{(2),a}(q^2) - \hat{\Pi}_S^{(2),a}(q^2) \right) = 0. \quad (6)$$

In this difference the $\ln(-z)$ terms cancel for $z \rightarrow 0$ which makes it possible to demand this QED-like renormalization condition. Alternatively one could use the $\overline{\text{MS}}$ scheme where only the $1/\epsilon$ poles are subtracted.

An important ingredient for the Padé approximation is the expansion of $\Pi_S^{(2),a}(q^2)$ for small external momentum. It is obtained by applying the so-called hard mass procedure [10] which provides a consistent expansion in q^2/m^2 :

$$\Pi_S^{(2),a}(q^2) = \frac{3}{16\pi^2} \sum_{n \geq 0} C_{S,n}^{(2),a} z^n. \quad (7)$$

The first eight coefficients have been evaluated:

$$\begin{aligned} C_{S,0}^{(2),a} &= K^a + \frac{37}{6} l_{qm} - l_{qm}^2 \\ C_{S,1}^{(2),a} &= \frac{471631}{311040} + \frac{5215}{13824} \zeta_3 - \frac{56}{81} l_{qm} \\ C_{S,2}^{(2),a} &= \frac{1178417}{8064000} + \frac{18179}{92160} \zeta_3 - \frac{14}{75} l_{qm} \\ C_{S,3}^{(2),a} &= -\frac{15527720419}{5120962560000} + \frac{1811719}{14745600} \zeta_3 - \frac{13312}{165375} l_{qm} \\ C_{S,4}^{(2),a} &= -\frac{23054974995287}{811160469504000} + \frac{5965963}{70778880} \zeta_3 - \frac{7696}{178605} l_{qm} \\ C_{S,5}^{(2),a} &= -\frac{735623850793897673}{23817834479222784000} + \frac{16260413}{264241152} \zeta_3 - \frac{6600448}{252130725} l_{qm} \\ C_{S,6}^{(2),a} &= -\frac{1301167265336208772211}{46002446022727434240000} + \frac{425212357}{9059696640} \zeta_3 - \frac{3007168}{173918745} l_{qm} \\ C_{S,7}^{(2),a} &= -\frac{11171249029492611725205473}{450455951454547036078080000} + \frac{193004110999}{5218385264640} \zeta_3 - \frac{132788224}{10956880935} l_{qm}, \end{aligned} \quad (8)$$

with $\zeta_3 \approx 1.202056903$ and $l_{qm} = \ln(-q^2/m^2)$. K^a is a constant whose numerical value will be given below.

A stringent constraint both for the real and imaginary part of $\Pi_S^{(2),a}(q^2)$ is set by the expansion for large external momentum. Recently, the large momentum procedure has been applied leading to the result [8]¹:

$$\begin{aligned} \Pi_S^{(2),a}(q^2) &= \frac{3}{16\pi^2} \left\{ K^a + \frac{185}{16} - \frac{385}{288} \zeta_3 + 21 \zeta_3 \frac{m^2}{q^2} \right. \\ &\quad + \left(\frac{m^2}{q^2} \right)^2 \left[-\frac{80}{3} \zeta_3 + \frac{320}{3} \zeta_5 \right] \\ &\quad + \left(\frac{m^2}{q^2} \right)^3 \left[\frac{380}{3} - 64 \zeta_3 + \left(\frac{296}{3} - 32 \zeta_3 \right) l_{qm} + 24 l_{qm}^2 \right] \\ &\quad \left. + \left(\frac{m^2}{q^2} \right)^4 \left[-\frac{3271}{243} - \frac{416}{9} \zeta_3 + \left(\frac{280}{27} + 32 \zeta_3 \right) l_{qm} + \frac{410}{27} l_{qm}^2 - \frac{176}{27} l_{qm}^3 \right] \right\} \end{aligned}$$

¹In [8] the results are listed in the $\overline{\text{MS}}$ scheme.

$$\begin{aligned}
& + \left(\frac{m^2}{q^2} \right)^5 \left[-\frac{395921}{2916} - \frac{5584}{27} \zeta_3 \right. \\
& \quad \left. + \left(\frac{4111}{54} + \frac{160}{3} \zeta_3 \right) l_{qm} + \frac{1340}{9} l_{qm}^2 - \frac{1660}{81} l_{qm}^3 \right] \\
& + \left(\frac{m^2}{q^2} \right)^6 \left[-\frac{105441373}{101250} - \frac{2420}{3} \zeta_3 \right. \\
& \quad \left. + \left(-\frac{6044237}{40500} + 112 \zeta_3 \right) l_{qm} + \frac{1177331}{1350} l_{qm}^2 - \frac{15542}{135} l_{qm}^3 \right] \Big\} + \dots, \quad (9)
\end{aligned}$$

with ζ_3 defined above and $\zeta_5 \approx 1.036927755$.

The logarithms in Eq. (8) are due to the massless cuts and do not appear in the non-singlet diagrams [3]. They spoil the procedure for constructing the Padé approximants developed in [3]. Therefore, instead of dealing with the full polarization function, one may use Eq. (5) and consider the following quantity:

$$\Pi_{S,mod}^{(2),a}(q^2) = \Pi_S^{(2),a}(q^2) - \hat{\Pi}_S^{(2),a}(q^2). \quad (10)$$

According to the definition of $\hat{\Pi}_S^{(2),a}(q^2)$ the $\ln(-z)$ -terms from the low energy expansion of $\Pi_S^{(2),a}(q^2)$ are exactly canceled. Above $z = 1$, the imaginary part on the r.h.s. of Eq. (10) is determined by $\Pi_S^{(2),a}(q^2)$ alone. This means that for $z > 1$, $\Pi_{S,mod}^{(2),a}(q^2)$ contains all possible cuts of the double-triangle diagrams and one should subtract the massless ones by using $R_{sb}^{(2),a}(s)$ in the region $s > 4m^2$ to get the production cross section for massive quarks.

An analytic formula for $R_{sb}^{(2),a}(s)$ is available [11]². Nevertheless it is not possible to solve the dispersion integral in Eq. (10) analytically. On the other hand a purely numerical integration is excluded as the result contains $\ln(-z)$ terms for $z \rightarrow 0$ which makes an expansion of the integrand with subsequent integration impossible. Let us therefore briefly describe the method we used for evaluation of Eq. (5).

One may write $R_{sb}^{(2),a}(s)$ as (recall Eq. (1))

$$R_{sb}^{(2),a}(s) = 3 \frac{3}{2} \ln(4r) + \tilde{R}_{sb}^{(2),a}(s). \quad (11)$$

Then $\tilde{R}_{sb}^{(2),a}(s)$ has a very simple limiting behaviour. For $s \rightarrow 0$ it reads

$$\tilde{R}_{sb}^{(2),a}(s) = 3 \left[-\frac{37}{8} + \frac{14}{27} r + \frac{7}{50} r^2 + \dots \right], \quad (12)$$

where the dots represent higher orders in r . The expansion of $\tilde{R}_{sb}^{(2),a}(s)$ around $\sqrt{s} = 2m$ leads to

²In [11] a different kinematical region was considered. However, we continued the result to the region under consideration by using the translation table given in the appendix of [11].

$$\begin{aligned}\tilde{R}_{sb}^{(2),a}(s) = & 3 \left[-\frac{19}{8} - \frac{3}{2}\zeta_2 + \frac{7}{8}\zeta_3 + (1-r) \left(\frac{1}{2} - 3\zeta_2 + \frac{7}{4}\zeta_3 \right) \right. \\ & \left. + \left(\sqrt{1-r} \right)^3 \left(2\pi - \frac{4}{3}\pi \ln 2 \right) + \dots \right],\end{aligned}\quad (13)$$

i.e., in this limit $\tilde{R}_{sb}^{(2),a}(s)$ is a series in $\sqrt{1-r}$. Provided with this information we split the integral in Eq. (5) into three parts:

$$\int_0^1 dr \frac{R_{sb}^{(2),a}(s)}{r-z} = \int_0^1 dr \frac{3 \frac{3}{2} \ln(4r)}{r-z} + \int_0^\delta dr \frac{\tilde{R}_{sb}^{(2),a}(s)}{r-z} + \int_\delta^1 dr \frac{\tilde{R}_{sb}^{(2),a}(s)}{r-z} \quad (14)$$

and replace in a second step $\tilde{R}_{sb}^{(2),a}(s)$ in the interval $[0, \delta]$ by the expansion in (12), in the interval $[\delta, 1]$ by the one in (13). It turns out that the inclusion of the first 100 terms in the small energy expansion and the first 40 terms in the expansion around $r = 1$ leads to stable results in the range $\delta = 0.65 \dots 0.80$ with an accuracy of 13 to 14 digits. We will not quote numbers for the full $\hat{\Pi}_S^{(2),a}(q^2)$ but only for the constant K^a appearing in Eqs. (8) and (9):

$$K^a = -9.08040684374401 \dots \quad (15)$$

The third kinematic region to be used for the Padé procedure is the threshold for the production of two massive quarks, $z \rightarrow 1$. In this region $\Pi_S^{(2),a}(q^2)$ gets contributions from two sources: the cuts involving massive quarks and $R_{sb}^{(2),a}(s)$. It is strongly expected that the former starts at least with a term proportional to v in analogy to the non-singlet axial-vector correlator which follows the P -wave scattering solution of the Coulomb potential. $R_{sb}^{(2),a}(s)$ on the other hand has a smooth behaviour for $s \rightarrow 4m^2$. For $z < 1$, $\Pi_{S,mod}^{(2),a}(q^2)$ is constructed in such a way that its imaginary part vanishes. However, the leading contribution of $\Pi_{S,mod}^{(2),a}(q^2)$ for $z \rightarrow 1^+$ is given by

$$\Pi_{S,mod}^{(2),a}(q^2) = \frac{3}{16\pi^2} \ln \left(\frac{1}{1-z} \right) \left(-\frac{19}{6} + 4 \ln 2 - 2\zeta_2 + \frac{7}{6}\zeta_3 \right) + \dots, \quad (16)$$

where the ellipses represent sub-leading terms in $(1-z)$.

The construction of the Padé approximations divides naturally into four steps (for more detail we refer to [3]): First, the threshold contribution has to be subtracted in all kinematical regions in order to have a polarization function that has a vanishing imaginary part for $z \rightarrow 1$. Then, a new polarization function, $\tilde{\Pi}_{S,mod}^{(2),a}(q^2)$, is constructed whose high energy expansion contains no logarithmic terms any more. This must be done carefully in order not to destroy the behavior for $z \rightarrow 0$ and $z \rightarrow 1$. In a third step the conformal mapping [4]

$$z = \frac{4\omega}{(1+\omega)^2} \quad (17)$$

is used to transform the q^2 plane into the interior of the unit circle. Finally, a Padé improvement is performed in the new variable, ω .

In [3] only the constant and the m^2/q^2 corrections in the high energy expansion have been included into the analysis. For the singlet diagrams meanwhile terms up to $\mathcal{O}((m^2/q^2)^6)$ are available. This makes it necessary to modify the definition of the function $P(\omega)$ for which the Padé approximation is performed. The natural extension of the definition given in [3] reads:

$$P_n(\omega) = \frac{(4\omega)^{n-1}}{(1+\omega)^{2n}} \left(\tilde{\Pi}_{S,mod}^{(2),a}(q^2) - \sum_{j=0}^{n-1} \frac{1}{j!} \left(\frac{d^j}{d(1/z)^j} \tilde{\Pi}_{S,mod}^{(2),a}(q^2) \right) \Big|_{z=-\infty} \right) \frac{(1+\omega)^{2j}}{(4\omega)^j}, \quad (18)$$

where the index $n \geq 1$ indicates that the mass corrections of order $(m^2/q^2)^n$ are included. The Padé approximants

$$[i/j](\omega) = \frac{a_0 + a_1\omega + \dots + a_i\omega^i}{1 + b_1\omega + \dots + b_j\omega^j} \quad (19)$$

are then constructed from $P_n(-1)$ and $P_n^{(k)}(0)$, ($k = 0, 1, \dots, n + n_0 - 1$), where n_0 is the number of moments (see Eq. (8)) used for the construction of the Padé approximation and $P_n^{(k)}(0) = \frac{d^k}{d\omega^k} P_n(\omega)|_{\omega=0}$. Taking into account all available information, i.e. $n = 6$ and $n_0 = 7$, it is possible to construct approximants like $[7/6]$, $[6/7]$ or $[8/5]$. However, it turns out that the construction of $P_n^{(k)}(0)$ for large values of k suffers from huge cancellations. It is therefore necessary to evaluate the expressions in Eq. (14) with highest possible accuracy in order to arrive at reliable results for high-order Padé approximations. After all, the above mentioned 13 to 14 digits are enough to get stable results. Of course, also lower order Padé's have been evaluated both for consistency checks and to examine the convergence properties. We should mention that some of the Padé approximants develop poles for $|\omega| < 1$ which result in poles in the physical z plane. Since this is not acceptable, only Padé approximants free from poles in the physical region are considered in the discussion of Section IV. We refrain from listing explicit formulae for $\Pi_S^{(2),a}(q^2)$ at this point and instead present in Section IV results for the imaginary part, $R_S^{(2),a}(s)$.

III. SCALAR AND PSEUDO-SCALAR CASE

It is now straightforward to extend the procedure described above to the scalar and pseudo-scalar case. Here, in contrast to the singlet axial-vector contribution only the diagram with two massive triangles contributes. However, the cut through the two gluons does not vanish as it was the case for the axial-vector coupling, so that again there is a cut starting at $z = 0$.

The polarization functions are defined through (κ stands for s and p , denoting the scalar and pseudo-scalar case, respectively):

$$q^2 \Pi^\kappa(q^2) = i \int dx e^{iqx} \langle 0 | T j^\kappa(x) j^\kappa(0) | 0 \rangle, \quad (20)$$

$$R^\kappa(s) = 8\pi \text{Im} \Pi^\kappa(q^2 = s + i\epsilon), \quad (21)$$

where the currents are given by $j^s = \bar{\psi}\psi$ and $j^p = i\bar{\psi}\gamma_5\psi$. As for j^p one again has to deal with γ_5 in $D \neq 4$ dimensions, we again adopt the definition of [7], referring for details to [12].

In analogy to (5) we define:

$$\hat{\Pi}_S^\kappa(q^2) = \frac{1}{8\pi^2} \int_0^1 dr \frac{R_{gg}^{(2),\kappa}(s)}{r-z}. \quad (22)$$

$R_{gg}^{(2),\kappa}(s)$ corresponds to the two gluon cut actually describing the Born decay of a scalar or pseudo-scalar Higgs boson to gluons [13,14]:

$$R_{gg}^{(2),s} = \frac{3}{2r} \left(1 + \frac{r-1}{r} f(r)\right)^2, \quad R_{gg}^{(2),p} = \frac{3}{2r} (f(r))^2, \quad (23)$$

with

$$f(r) = \begin{cases} \arcsin^2(\sqrt{r}), & r \leq 1 \\ -\frac{1}{4} \left[\log \frac{1+\sqrt{1-1/r}}{1-\sqrt{1-1/r}} - i\pi \right]^2, & r > 1. \end{cases} \quad (24)$$

Although these functions are quite simple an analytic integration is hard to perform. So we adopt the same procedure as for the axial-vector case and expand $R_{gg}^{(2),\kappa}(s)$ for $s \rightarrow 0$, where we take 200 terms into account, and for $s \rightarrow 4m^2$, where 50 terms are enough to get a precision of 17 to 18 digits in the interval $\delta \in [0.65, 0.80]$.

In analogy to Eq. (6) the overall renormalization condition reads:

$$\lim_{q^2 \rightarrow 0} \left(\Pi_S^{(2),\kappa}(q^2) - \hat{\Pi}_S^{(2),\kappa}(q^2) \right) = 0. \quad (25)$$

In this scheme, the low-energy expansion of $\Pi_S^{(2),\kappa}(q^2)$ looks as follows:

$$\begin{aligned} C_{S,0}^{(2),s} &= K^s \\ C_{S,1}^{(2),s} &= \frac{4609}{2880} + \frac{721}{1152} \zeta_3 - \frac{4}{9} l_{qm} \\ C_{S,2}^{(2),s} &= \frac{2719121}{5806080} + \frac{10871}{36864} \zeta_3 - \frac{28}{135} l_{qm} \\ C_{S,3}^{(2),s} &= \frac{519513881}{3483648000} + \frac{1330021}{7372800} \zeta_3 - \frac{1543}{14175} l_{qm} \\ C_{S,4}^{(2),s} &= \frac{2460910303}{57480192000} + \frac{50939}{409600} \zeta_3 - \frac{904}{14175} l_{qm} \\ C_{S,5}^{(2),s} &= \frac{8958934229477}{2929190584320000} + \frac{2526649}{27525120} \zeta_3 - \frac{221416}{5457375} l_{qm} \\ C_{S,6}^{(2),s} &= -\frac{37498822356303853}{2999491158343680000} + \frac{5991294557}{84557168640} \zeta_3 - \frac{5844896}{212837625} l_{qm} \\ C_{S,7}^{(2),s} &= -\frac{112110439141686419569}{61189619630211072000000} + \frac{245566743541}{4348654387200} \zeta_3 - \frac{20750416}{1064188125} l_{qm} \end{aligned}$$

$$C_{S,8}^{(2),s} = -\frac{14445289941190001679673}{723397280961606451200000} + \frac{1604104532801}{34789235097600} \zeta_3 - \frac{140071424}{9741414375} l_{qm}, \quad (26)$$

$$\begin{aligned} C_{S,0}^{(2),p} &= K^p \\ C_{S,1}^{(2),p} &= \frac{55}{16} + \frac{175}{96} \zeta_3 - l_{qm} \\ C_{S,2}^{(2),p} &= \frac{20143}{11520} + \frac{5047}{4608} \zeta_3 - \frac{2}{3} l_{qm} \\ C_{S,3}^{(2),p} &= \frac{2468869}{2419200} + \frac{3969}{5120} \zeta_3 - \frac{7}{15} l_{qm} \\ C_{S,4}^{(2),p} &= \frac{920009009}{1393459200} + \frac{974281}{1638400} \zeta_3 - \frac{328}{945} l_{qm} \\ C_{S,5}^{(2),p} &= \frac{5898858645227}{12875563008000} + \frac{753259}{1572864} \zeta_3 - \frac{3832}{14175} l_{qm} \\ C_{S,6}^{(2),p} &= \frac{5523023003231}{16531587072000} + \frac{11702895}{29360128} \zeta_3 - \frac{3776}{17325} l_{qm} \\ C_{S,7}^{(2),p} &= \frac{63171728144529503}{249957596528640000} + \frac{205215857}{603979776} \zeta_3 - \frac{4266896}{23648625} l_{qm} \\ C_{S,8}^{(2),p} &= \frac{481264894165689829721}{2447584785208442880000} + \frac{513043585411}{1739461754880} \zeta_3 - \frac{32459264}{212837625} l_{qm}, \end{aligned} \quad (27)$$

where $\Pi_S^{(2),\kappa}(q^2)$ and $C_{S,n}^{(2),\kappa}$ are defined in analogy to Eqs. (3) and (7), and

$$K^s = 0.62280338337755 \dots, K^p = 1.81359971877046 \dots. \quad (28)$$

The high energy expansion terms up to $\mathcal{O}(1/z^4)$ are already listed in [12] in the $\overline{\text{MS}}$ scheme. We have added the $(m^2/s)^5$ and $(m^2/s)^6$ mass correction terms. In the renormalization scheme defined in Eq. (25) the result reads ($l_{q\mu} = \ln(-q^2/\mu^2)$, with μ being the renormalization scale):

$$\begin{aligned} \Pi_S^{(2),s} &= \frac{3}{16\pi^2} \left\{ K^s - \frac{5}{8} - \frac{49}{16} \zeta_3 + \frac{m^2}{q^2} \left[68 + 2 \zeta_3 - 20 \zeta_5 - 24 l_{q\mu} \right] \right. \\ &\quad + \left(\frac{m^2}{q^2} \right)^2 \left[-84 + 8 \zeta_3 + 160 \zeta_5 + (-36 + 72 \zeta_3) l_{qm} \right] \\ &\quad + \left(\frac{m^2}{q^2} \right)^3 \left[\frac{37}{8} - 62 \zeta_3 + 320 \zeta_5 + \left(-\frac{3}{4} - 36 \zeta_3 \right) l_{qm} + 33 l_{qm}^2 + 12 l_{qm}^3 \right] \\ &\quad + \left(\frac{m^2}{q^2} \right)^4 \left[\frac{178423}{243} - \frac{4472}{9} \zeta_3 + \left(\frac{22289}{81} + 16 \zeta_3 \right) l_{qm} \right. \\ &\quad \left. \left. - 26 l_{qm}^2 - \frac{28}{3} l_{qm}^3 \right] \right. \\ &\quad \left. + \left(\frac{m^2}{q^2} \right)^5 \left[\frac{12256783}{62208} - \frac{8551}{18} \zeta_3 + \left(\frac{1594853}{5184} + 46 \zeta_3 \right) l_{qm} \right] \right\} \end{aligned}$$

$$\begin{aligned}
& + \frac{1697}{72} l_{qm}^2 + \frac{236}{9} l_{qm}^3 \Big] \\
& + \left(\frac{m^2}{q^2} \right)^6 \left[\frac{474209987}{1620000} - \frac{58672}{225} \zeta_3 + \left(\frac{56656079}{202500} + \frac{576}{5} \zeta_3 \right) l_{qm} \right. \\
& \quad \left. - \frac{50407}{90} l_{qm}^2 + \frac{5758}{27} l_{qm}^3 \right] \Big\} + \dots , \tag{29} \\
\Pi_S^{(2),p} = & \frac{3}{16\pi^2} \Big\{ K^p - \frac{21}{4} \zeta_3 + \frac{m^2}{q^2} \left[-16 \zeta_3 - 20 \zeta_5 \right] \\
& + \left(\frac{m^2}{q^2} \right)^2 \left[-44 + 24 \zeta_3 + (-12 - 72 \zeta_3) l_{qm} \right] \\
& + \left(\frac{m^2}{q^2} \right)^3 \left[\frac{221}{8} + 114 \zeta_3 + \left(-\frac{363}{4} - 36 \zeta_3 \right) l_{qm} - 63 l_{qm}^2 - 12 l_{qm}^3 \right] \\
& + \left(\frac{m^2}{q^2} \right)^4 \left[\frac{68146}{243} + \frac{1288}{9} \zeta_3 + \left(\frac{7727}{81} - 80 \zeta_3 \right) l_{qm} - 86 l_{qm}^2 - 44 l_{qm}^3 \right] \\
& + \left(\frac{m^2}{q^2} \right)^5 \left[\frac{12754021}{20736} + \frac{787}{6} \zeta_3 + \left(\frac{1164055}{1728} - 210 \zeta_3 \right) l_{qm} \right. \\
& \quad \left. - \frac{7}{8} l_{qm}^2 - 172 l_{qm}^3 \right] \\
& + \left(\frac{m^2}{q^2} \right)^6 \left[\frac{11857111}{22500} - \frac{15108}{25} \zeta_3 + \left(\frac{40729829}{15000} - \frac{3024}{5} \zeta_3 \right) l_{qm} \right. \\
& \quad \left. + \frac{11417}{10} l_{qm}^2 - 738 l_{qm}^3 \right] \Big\} + \dots . \tag{30}
\end{aligned}$$

It should be noted that in the scalar case the singlet polarization function explicitly depends on the renormalization scale μ . For the approximation procedure the choice $\mu^2 = m^2$ will be adopted. The imaginary part, however, is independent of μ .

The analogue of Eq. (10) reads

$$\Pi_{S,mod}^{(2),\kappa}(q^2) = \Pi_S^{(2),\kappa}(q^2) - \hat{\Pi}_S^{(2),\kappa}(q^2). \tag{31}$$

The leading threshold term of this function both for $\kappa = s$ and p will be determined in complete analogy to the axial-vector case (see Eq. (16)), despite the fact that for the non-singlet part in the pseudo-scalar case it originates from the S -wave solution of the Coulomb potential. If by this procedure an essential contribution to the threshold part is missing, different Padé results should develop a large spread close to $v = 0$. One obtains

$$\Pi_{S,mod}^{(2),s}(q^2) = \frac{3}{16\pi^2} \ln \left(\frac{1}{1-z} \right) + \dots, \quad \Pi_{S,mod}^{(2),p}(q^2) = \frac{3}{16\pi^2} \ln \left(\frac{1}{1-z} \right) \frac{\pi^4}{16} + \dots. \tag{32}$$

The approximation procedure is applied in complete analogy to the axial-vector correlator. As for the scalar and pseudo-scalar case also the eighth moment, $C_{S,8}^{(2),s/p}$, is available, Padé's like [7/7], [8/6] or [6/8] may be evaluated.

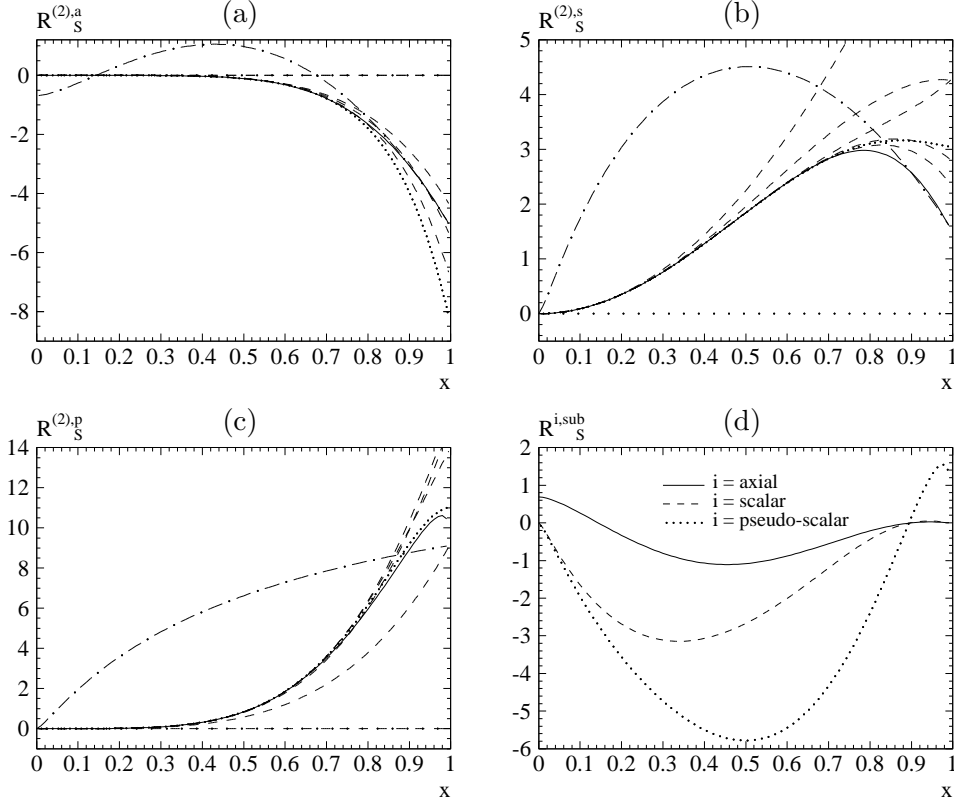


FIG. 2. The imaginary parts $R_S^{(2),a}$, $R_S^{(2),s}$ and $R_S^{(2),p}$ of (a) the axial-vector, (b) scalar and (c) pseudo-scalar singlet diagrams, respectively. For the abscissa the variable $x = 2m/\sqrt{s}$ is chosen. Solid line: Padé result; wide dots, dashes and narrow dots: $(m^2/q^2)^n$ -expansion for $n = 0$, $n = 1, \dots, 5$ and $n = 6$, respectively; dash-dotted line: purely massless cuts $R_{S_b}^{(2),a}$, $R_{gg}^{(2),s}$ and $R_{gg}^{(2),p}$. (d) shows the difference between the solid and the dashed dotted line (i.e., the contribution of the massive quarks) of (a), (b) and (c) as solid, dashed and dotted line, respectively.

IV. RESULTS

In Fig. 2 (a)–(c) the results for the imaginary part of $\Pi_S^{(2),a}$, $\Pi_S^{(2),s}$ and $\Pi_S^{(2),p}$ (solid lines), together with the first seven terms of the high energy expansion (dashed and dotted lines) are shown as functions of $x = 2m/\sqrt{s}$. Recall that in the displayed region, $0 < x < 1$, $\text{Im}\Pi_S^{(2)} = \text{Im}\Pi_{S,\text{mod}}^{(2)}$. Therefore, if one is interested, e.g., in (inclusive) production of the heavy quarks only, the corresponding massless cuts (depicted as dash-dotted lines) have to be subtracted. The resulting curves are shown in Fig. 2 (d).

As was already pointed out in [8], the imaginary part of the axial-vector singlet contribution starts at $\mathcal{O}(m^6/s^3)$. Therefore, $R_S^{(2),a}$ is rather small below $x = 1/2$. On the other hand, above this value the four-particle threshold at $\sqrt{s} = 4m$ is expected to in-

hibit convergence of the high energy expansion. However, there is still an agreement of the $(m^2/s)^6$ -terms with the semi-analytical Padé result up to $x \approx 0.7$. Also in the scalar and pseudo-scalar case convergence of the high energy expansion is quite fast up to $x \approx 0.7 \dots 0.8$. For the pseudo-scalar case even very close to threshold the difference to the Padé result is rather small.

Minor differences among the various Padé approximations are visible only close to threshold. In Fig. 3 (a)–(c) for each correlator 30 Padé approximants with different input from $q^2 \rightarrow 0$ and $q^2 \rightarrow -\infty$ are plotted as functions of the quark velocity $v = \sqrt{1 - 4m^2/s}$. The dotted curve shows the $(m^2/s)^6$ -terms of the high energy expansion for comparison. The spread of the different Padé approximations serves as a measure for the uncertainty of the procedure. The dash-dotted line again corresponds to the purely massless cuts which largely dominate the singlet contribution in all three cases. For the axial-vector and the scalar case the differences $R_S^{(2),a} - R_{Sb}^{(2),a}$, respectively, $R_S^{(2),s} - R_{gg}^{(2),s}$ are remarkably small below $v = 0.5$ which confirms our previous assumptions on the threshold behavior in these cases (see Fig. 3 (d)). As was expected the analogue quantity in the pseudo-scalar case grows steeper for $v \rightarrow 0$, but still the stability of the Padé result justifies the threshold assumption. We even modified artificially Eq. (32) by $\pm 10\%$ and observed a drastic destabilisation of the Padé approximants. This also gives quite some confidence to the ansatz for $\Pi_S^{(2),p}$ at threshold.

In the following handy approximation formulae for the imaginary parts $R_S^{(2),a}$, $R_S^{(2),s}$ and $R_S^{(2),p}$ are given. To keep the formulae as short as possible a Padé approximant containing the high energy input up to $\mathcal{O}(m^2/s)$ is selected. After subtraction of the known analytic results the (small) remainder, which vanishes both for $v = 0$ and $v = 1$ is approximated using Legendre polynomials. The results read:

$$\begin{aligned}
R_S^{(2),a} = & -\frac{57}{8} + \frac{9}{2} \ln 4 - \frac{9}{2} \zeta_2 + \frac{21}{8} \zeta_3 + v \left(\frac{171}{16} - \frac{27}{4} \ln 4 \right) + v^3 \left(-\frac{57}{16} + \frac{9}{4} \ln 4 \right) \\
& + \left(\frac{27}{4} v - \frac{9}{4} v^3 \right) \zeta_2 + \left(-\frac{63}{16} v + \frac{21}{16} v^3 \right) \zeta_3 \\
& + 12 \left(\frac{m^2}{s} \right)^{3/2} (v^4 - 2v^2)^4 \\
& + 50p^{3/2}(1-p) [-0.0789 P_0(p) - 0.0869 P_1(p) + 0.1099 P_2(p)], \tag{33}
\end{aligned}$$

$$\begin{aligned}
R_S^{(2),s} = & \frac{3}{2} + \frac{27}{4} v - \frac{33}{4} v^3 \\
& + 3 \left(\frac{m^2}{s} \right)^{3/2} (v^4 - 2v^2)^4 \\
& + 50p^{3/2}(1-p) [-0.193 P_0(p) + 0.111 P_1(p) + 0.0277 P_2(p)], \tag{34}
\end{aligned}$$

$$\begin{aligned}
R_S^{(2),p} = & \pi^4 \left(\frac{3}{32} - \frac{9}{64} v + \frac{3}{64} v^3 \right) \\
& - 35 \left(\frac{m^2}{s} \right)^{3/2} (v^4 - 2v^2)^4
\end{aligned}$$

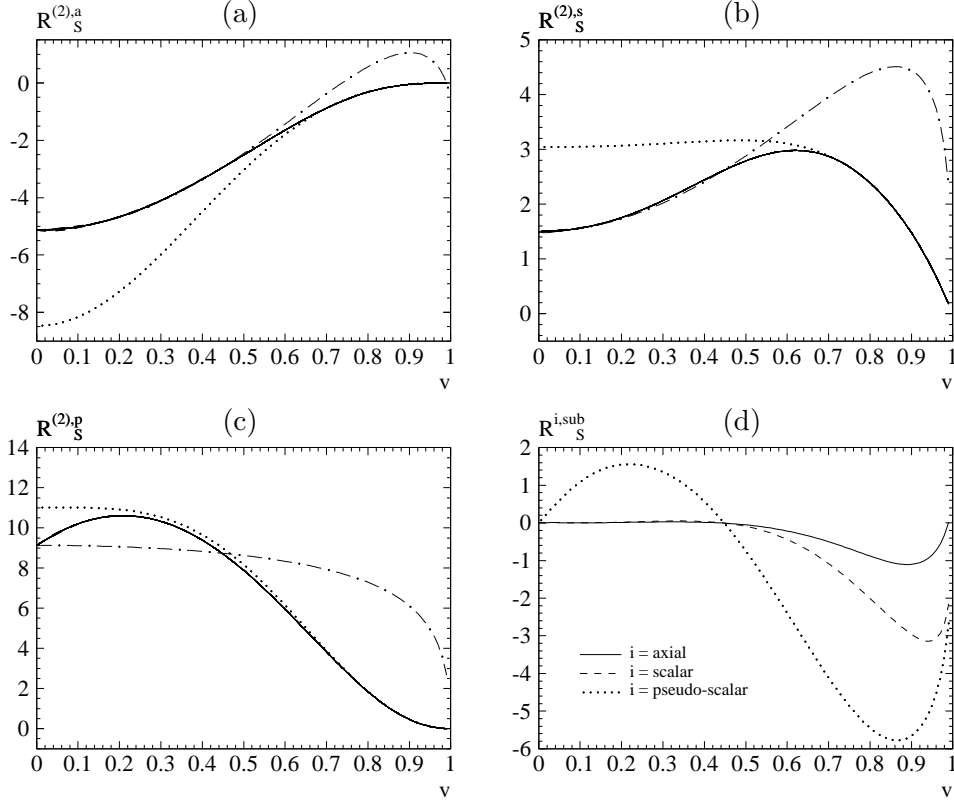


FIG. 3. $R_S^{(2),a}$, $R_S^{(2),s}$, $R_S^{(2),p}$ as functions of $v = \sqrt{1 - 4m^2/s}$. Solid and dashed lines: 30 different Padé curves; dotted: high energy expansion up to $(m^2/s)^6$; dash-dotted: purely massless cuts. (d) is the analogue of Fig. 2 (d), plotted over v .

$$+ 50p^{3/2}(1-p) [1.586 P_0(p) - 1.822 P_1(p) + 0.525 P_2(p)] , \quad (35)$$

with $p = (1-v)/(1+v)$. Note again that the corresponding massless cuts (see Eqs. (11) and (23)) have to be subtracted in order to find the rates for, e.g., $t\bar{t}$ production.

To summarize, the polarization functions for axial-vector, scalar and pseudo-scalar singlet current correlators have been computed. To this end the knowledge of $\Pi(q^2)$ for $q^2 \rightarrow 0$, $q^2 \rightarrow -\infty$ and $q^2 \rightarrow 4m^2$ has been exploited in combination with conformal mapping and Padé approximation. Results have been presented for the imaginary parts and handy approximation formulae have been provided. This completes the evaluation of three-loop polarization functions at $\mathcal{O}(\alpha_s^2)$ as in [3] the non-singlet contributions were considered.

Acknowledgments

We would like to thank B.K. Kniesl and J.H. Kühn for helpful discussions. MS appreciates the warm hospitality at the Institute for Theoretical Particle Physics at the University of Karlsruhe. This work was supported by BMBF under Contract 057KA92P, DFG under

Contract Ku 502/8-1 and INTAS under Contract INTAS-93-744-ext. RH thanks the “Landesgraduiertenförderung” at the University of Karlsruhe for financial support.

REFERENCES

- [1] K.G. Chetyrkin, J.H. Kühn and A. Kwiatkowski, *Phys. Rept.* **277** (1996) 189.
- [2] P.A. Baikov and D.J. Broadhurst, Presented at 4th International Workshop on Software Engineering and Artificial Intelligence for High Energy and Nuclear Physics (AIHENP95), Pisa, Italy, 3-8 April 1995. Published in Pisa AIHENP (1995) 167.
- [3] K.G. Chetyrkin, J.H. Kühn and M. Steinhauser, *Phys. Lett. B* **371** (1996) 93 *Nucl. Phys. B* **482** (1996) 213; *Nucl. Phys. B* **505** (1997) 40.
- [4] J. Fleischer and O.V. Tarasov, *Z. Phys. C* **64** (1994) 413.
- [5] D.J. Broadhurst, J. Fleischer and O.V. Tarasov, *Z. Phys. C* **60** (1993) 287.
- [6] D.J. Broadhurst et al., *Phys. Lett. B* **329** (1994) 103.
- [7] G. 't Hooft and M. Veltman, *Nucl. Phys. B* **44** (1972) 189;
P. Breitenlohner and D. Maison, *Commun. Math. Phys.* **52** (1977) 11.
- [8] R. Harlander and M. Steinhauser, Report Nos. MPI/PhT/97-66, TTP97-40, hep-ph/9710413, *Eur. Phys. J. C* (in press).
- [9] L.D. Landau, *Docl. Akad. Nauk USSR* **60** (1948) 207;
C.N. Yang, *Phys. Rev.* **77** (1950) 242.
- [10] For a review see: V.A. Smirnov, *Mod. Phys. Lett. A* **10** (1995) 1485.
- [11] B.A. Kniehl and J.H. Kühn, *Phys. Lett. B* **224** (1989) 229; *Nucl. Phys. B* **329** (1990) 547.
- [12] R. Harlander and M. Steinhauser, *Phys. Rev. D* **56** (1997) 3980.
- [13] J. Ellis, M.K. Gaillard and D.V. Nanopoulos, *Nucl. Phys. B* **106** (1976) 292.
- [14] A. Djouadi, M. Spira and P.M. Zerwas, *Phys. Lett. B* **311** (1993) 255.